

RFI Identification and Mitigation Using Simultaneous Dual Station Observations

N. D. R. Bhat

Massachusetts Institute of Technology, Haystack Observatory, Westford, MA 01886

J. M. Cordes

Astronomy Department and NAIC, Cornell University, Ithaca, NY 14853

S. Chatterjee

National Radio Astronomy Observatory, 1003 Lopezville Road, Socorro, NM 87801

T. J. W. Lazio

Remote Sensing Division, Naval Research Laboratory, Washington, DC 20375-5351

RFI mitigation is a critically important issue in radio astronomy using existing instruments as well as in the development of next-generation radio telescopes, such as the Square Kilometer Array (SKA). Most designs for the SKA involve multiple stations with spacings of up to a few thousands of kilometers and thus can exploit the drastically different RFI environments at different stations. As demonstrator observations and analysis for SKA-like instruments, and to develop RFI mitigation schemes that will be useful in the near term, we recently conducted simultaneous observations with Arecibo Observatory and the Green Bank Telescope (GBT). The observations were aimed at diagnosing RFI and using the mostly uncorrelated RFI between the two sites to excise RFI from several generic kinds of measurements such as giant pulses from Crab-like pulsars and weak HI emission from galaxies in bands heavily contaminated by RFI. This paper presents observations, analysis, and RFI identification and excision procedures that are effective for both time series and spectroscopy applications using multi-station data.

1. Introduction

Radio astronomers have begun to exploit the recent advent of wide-bandwidth receivers and spectrometers in order to obtain higher sensitivity as well as increased frequency coverage for spectroscopic observations. Consequently, observations often need to be made outside the (fairly narrow) frequency bands allocated to radio astronomy, forcing observers to explore various means of co-existence with other users of the spectrum, such as commercial and defense. In order to realize the full potential of these wide-bandwidth receivers and spectrometers, radio frequency interference (RFI) mitigation techniques will need to be devised and implemented at different stages within the signal path—at radio frequency (RF) front-end, pre-correlation and post-correlation.

Simultaneously, next generation radio telescopes are being designed and developed—such as the Allen Telescope Array (ATA), the Low Frequency Array (LOFAR), the Long Wavelength Array (LWA), and the Square Kilometer Array (SKA)—whose designs are radically different from most existing single-dish or interferometric telescopes. Naturally, they will need to deal with RFI environments that are drastically different from what observers have used so far. As such, RFI mitigation is recognized as a critically important issue in the development of these new class of instruments. Many of these next-generation radio telescopes (most notably the SKA, the LWA and to a lesser extent LOFAR) make use of array stations with separations as large as hundreds to even thousands of kilometers; the RFI environment can be expected to vary significantly depending on location of the station within the array, and the regulatory protection available in its vicinity. The same may apply to existing instruments such as the European VLBI

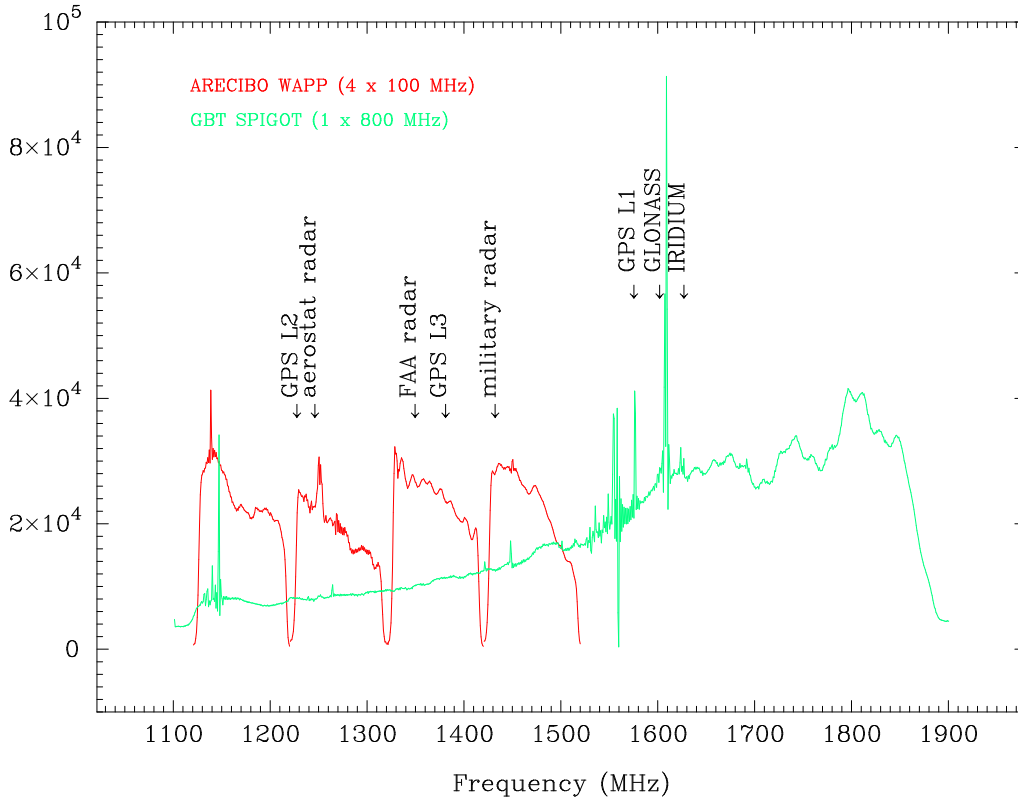


Figure 1. Example plots showing the instantaneous RFI environments in the L-band frequency range at the Arecibo and Green Bank Telescopes; these spectrometer bandshapes are from a short integration (1 s) of data taken on UGC 2339. Locations of some of the most prominent RFI sources are also marked.

Network (EVN) and the Very Long Baseline Array (VLBA), albeit they have much fewer number of stations and are primarily used in imaging applications. A design incorporating a large number of array stations at large distances from each other means that a possible RFI identification and mitigation technique is to exploit these large array station separations.

As demonstrator observations for SKA-like instruments, and also with the general goal of development of RFI excision methods that can potentially be applied to fast-sampled data in time and frequency, we recently conducted simultaneous observations with the Arecibo and Green Bank Telescopes. Data from such observations represent only a subclass of data obtainable from SKA-like instruments, and relevant for non-imaging type applications envisaged with the SKA, such as pulsar astronomy and transient searches. As part of these observations, data were gathered on the Crab pulsar, several beam areas on the galaxy M33, and the galaxies UGC 2339

and UGC 2602, at the L band frequency range. This paper will present observations, analysis, and RFI identification and excision procedures that are effective for both time series and spectroscopy applications using the dual-station data.

2. Arecibo-Green Bank Observations

Data used for the analysis presented in this paper are taken from observations made in November 2003 using the Arecibo and Green Bank Telescopes. At Arecibo, data were recorded using the wide-band correlation spectrometer, the Wideband Arecibo Pulsar Processor (WAPP, <http://www.naic.edu/~wapp>), four identical units of which were used to yield a total bandwidth of 400 MHz that spans the frequency range from 1120 to 1520 MHz. Data acquisition at the Green Bank Telescope (GBT) was done using the new GBT spectrometer SPIGOT card (<http://www.gb.nrao.edu/GBT>), which is capable

of a maximum bandwidth of 800 MHz, thus covering the frequency range from 1100 to 1900 MHz. As a result nearly 400 MHz of band is common to both the data sets.

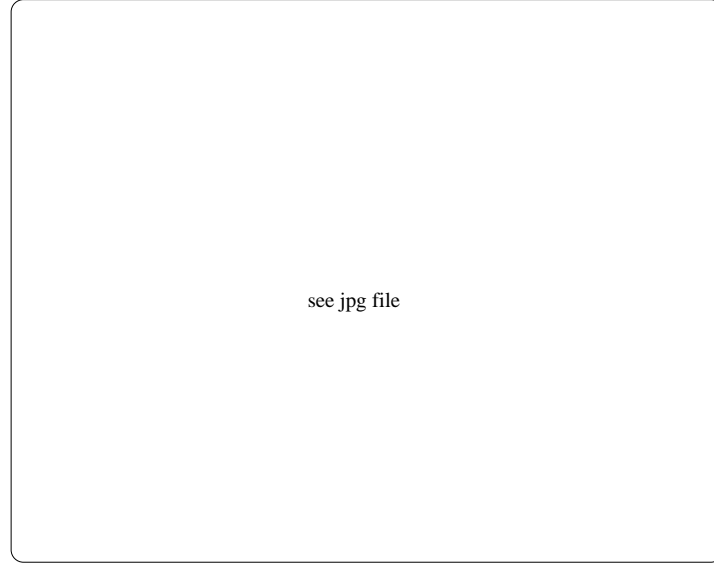


Figure 2. Schematic diagram illustrating the algorithm for identification and excision of RFI in fast-sampled spectrometer data. Data flow shown here follows the steps (1) to (6) as described in § 3.

In order to attempt our prime goal of exploring dual-station approach for better RFI excision techniques, specifically for spectroscopy applications, it is essential that data recording at the two telescopes use identical resolutions in time and frequency. This was feasible in our case owing to high level of flexibility and versatility offered by the WAPP systems, which allow the user to set arbitrary time and frequency resolutions. The observing parameters for each WAPP were chosen to exactly match that of the 800 MHz mode with the SPIGOT card. Data were taken at a sample interval of $82 \mu\text{s}$, 512 spectral channels spanning the composite 400 MHz band of the four WAPPs, and 1024 channels spanning the 800 MHz band of SPIGOT (i.e. a spectral resolution of 0.781 MHz for both data sets). Incidentally, by the time of these observations, Arecibo’s Gregorian sys-

tem was equipped with a new L-band wide receiver (<http://www.naic.edu/~astro/RXstatus/Lwide/Lwide.shtml>) whose design is identical to the one at the GBT. Thus our observing setups at the two telescopes are nearly identical, in terms of both spectrometer settings and choice of receivers, except for the obvious difference in primary beam widths and achievable sensitivities for the two telescopes.

In the remainder of the paper we describe some techniques useful for identification and excision of RFI in (i) fast-sampled spectrometer data, and (ii) dual-station time series data. Specifically, in § 3 we focus on a generic algorithm that can be applied to two-dimensional data in the time-frequency plane (i.e. dynamic spectrum) to generate RFI “masks” for input to a data processing pipeline, and in § 4 we leverage the utility of multiple-subband

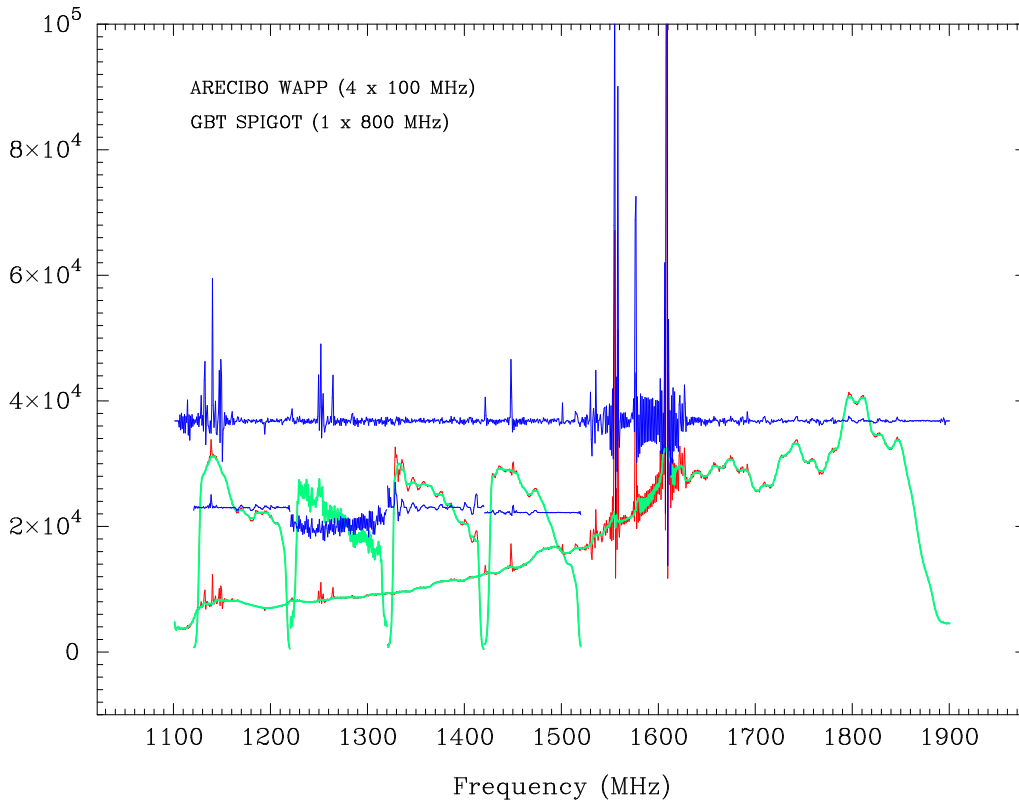


Figure 3. Example spectrometer bandshapes from a short integration (1 s) of data taken on the UGC 2339 galaxy; the raw bandshapes (red solid curves) are overplotted with the median-filtered, smoothed versions of the bands (green solid curves). The curves in blue represent the ratios of the raw data to smoothed data, and appropriately scaled for display.

and multiple-site approaches to differentiate impulsive RFI from real signal (events) in time series data.

3. Algorithm for Identification and Excision of RFI in Fast-sampled Spectrometer Data

Figure 1 shows examples of one-second averaged spectra obtained simultaneously in the L-band frequency range at Arecibo and Green Bank. Examination of such data as a function of time reveals the presence of a variety of RFI, ranging from RFI that is narrowband and persistent in nature (e.g. GPS modes L1, L2 and L3) to those that are strong and bursty (e.g. Iridium line at 1627 MHz). Their prominence can potentially lead to quite detrimental effects in applications such as pulsar data processing, and

may considerably limit the sensitivity achievable for spectroscopy observations.

We have devised an algorithm for the identification and excision of RFI in fast-sampled spectrometer data. Such data are especially sensitive to RFIs that are mostly strong and impulsive in nature. The general scheme involves applying a two-dimensional running median filter to the data (e.g. Ransom et al. 2004), followed by a series of thresholding and excision (flagging) stages, and possibly in multiple passes, in order to identify regions of data samples in the time-frequency plane that are corrupted by RFI. There are several adjustable parameters at various stages of the algorithm that can be optimized to yield the best results.

Note that for the sake of computational efficiency, as well as to ensure sufficient interference-to-noise ratio (INR), it is important to smooth and decimate (preferably in time) prior to application of the algorithm. In general, the decimation factor will depend

largely on the science application, the RFI environment at the telescope, and acceptable levels of data loss due to RFI excision. The algorithm essentially

steps through the sequence as listed below (see also Fig. 2):

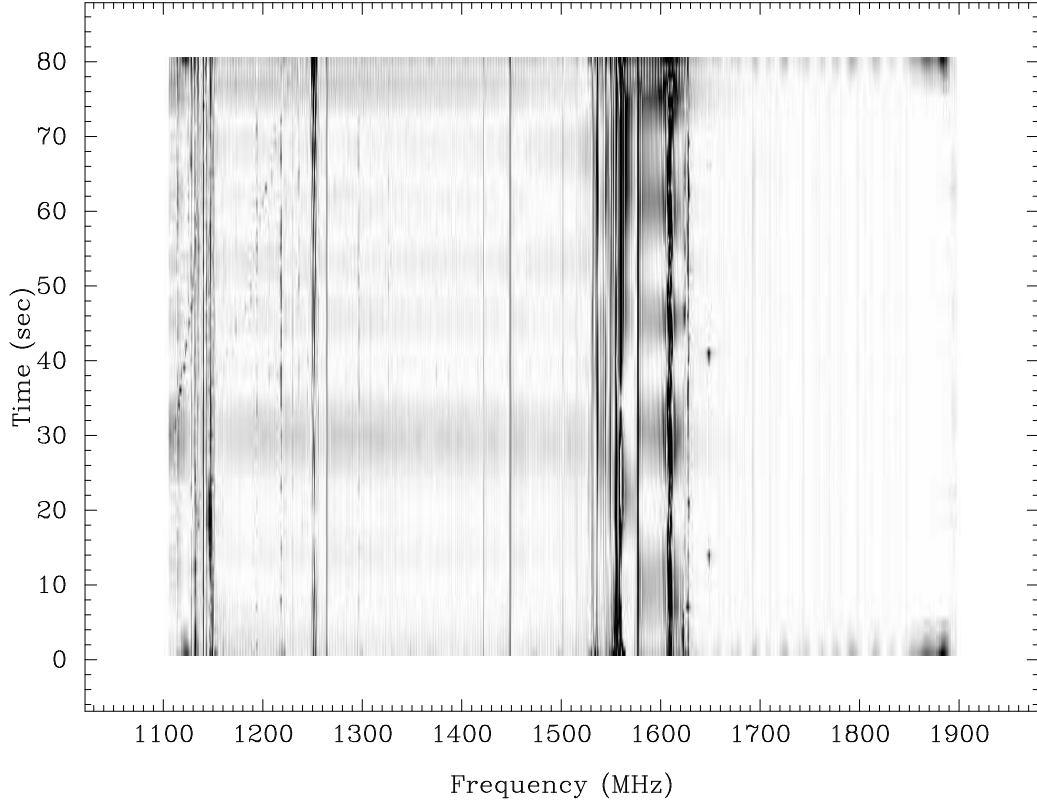


Figure 4. Gray scale plot showing the RFI-corrupted regions as identified by application of a two-dimensional median filter (5×5 pixels) to a short stretch of data taken on UGC 2339. The strength of the RFI (relative to the median bandpass level) is shown as a logarithmic gray scale, saturating (black) at 1.5 dB above the median power level.

(1) *Data decimation* : Start with full resolution (raw) data in the form of a dynamic spectrum, perform data decimation by doing short integrations of successive spectra in time (e.g., 0.1 to 1 s) to generate a time sequence of short-averaged spectra.

(2) *Median filtering* : Apply a two-dimensional median filter in time and frequency. This is an efficient method to identify RFI that is impulsive in nature, either in time or in frequency, or both. The ratio of the dynamic spectra of decimated raw data to the median-filtered data (Fig. 4) now forms the input for further stages.

(3) *Thresholding in frequency* : Identify and excise RFI that is persistent (and narrowband) in nature. This is achieved by averaging longer stretches of data, followed by computation of its statistics (in frequency), and application of suitable thresholding (e.g. 3σ) to identify spectral channels with persistent RFI.

(4) *Thresholding in time* : Identify and excise RFI that is broadband (and transient) in nature. For this, integrate the data over the full band (or multiple sub-bands), followed by computation of its statistics (in time), and application of thresholding.

(5) *Thresholding in time and frequency* : Identify and excise RFI that is localized in the time-frequency plane. Perform channel-wise computation of the statistics of the data, and apply thresholding in the

two-dimensional plane, to identify regions corrupted by RFI.

(6) *Multiple passes* : Iterate steps (3) to (5) until a satisfactory level of RFI excision is achieved.

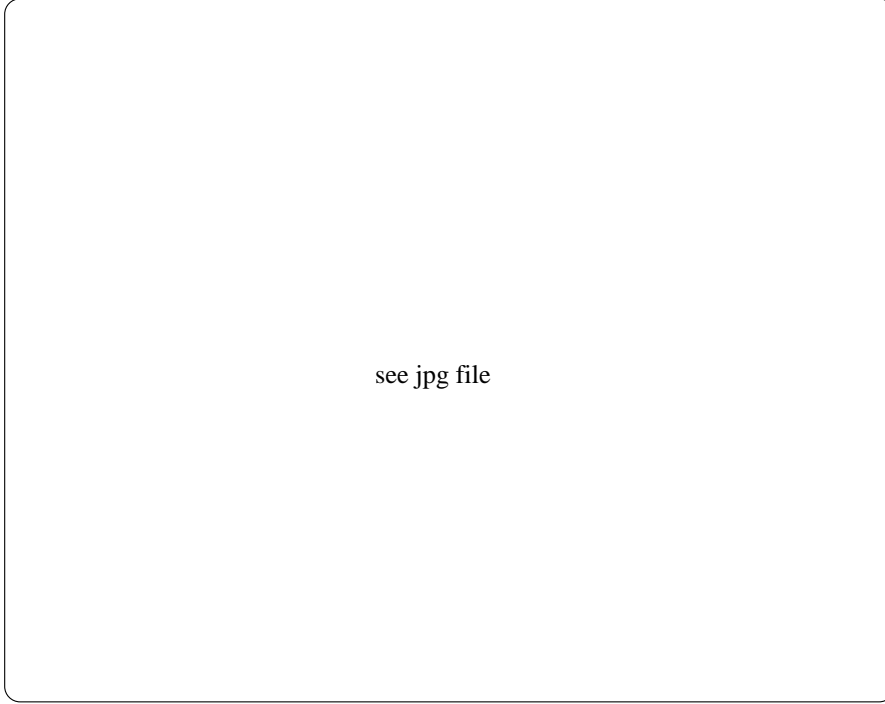


Figure 5. Gray scale plots illustrating the application of RFI identification and excision algorithm on spectroscopy data; the regions in red correspond to the data that are identified to be corrupted with RFI. Darker regions of the gray scale plot indicate the residual, unexcised RFI. The strength of the RFI is shown on a logarithmic scale, with the gray scale saturating (black) at 1.5 dB above the median power level.

Figures 3–6 show example plots that illustrate this method, using the UGC 2339 data taken with the GBT-SPIGOT system. Based on these and the above description, it is evident that the algorithm is primarily sensitive to impulsive type RFIs, either in time or frequency, such as narrowband bursts or persistent RFIs confined to a few spectral channels. The underlying assumption is that most real celestial

signals are characteristically different, and may even show signatures of dispersion and/or scattering (e.g. frequency structure from diffractive interstellar scintillation). While our method is primarily intended as an RFI finding algorithm (and not a transient event detection scheme), certain fast transients of broadband nature may be classified as RFI by this scheme. An ideal way to circumvent this may be to capture such “localized RFI events” and examine them in detail later on using appropriate matched-filter-like

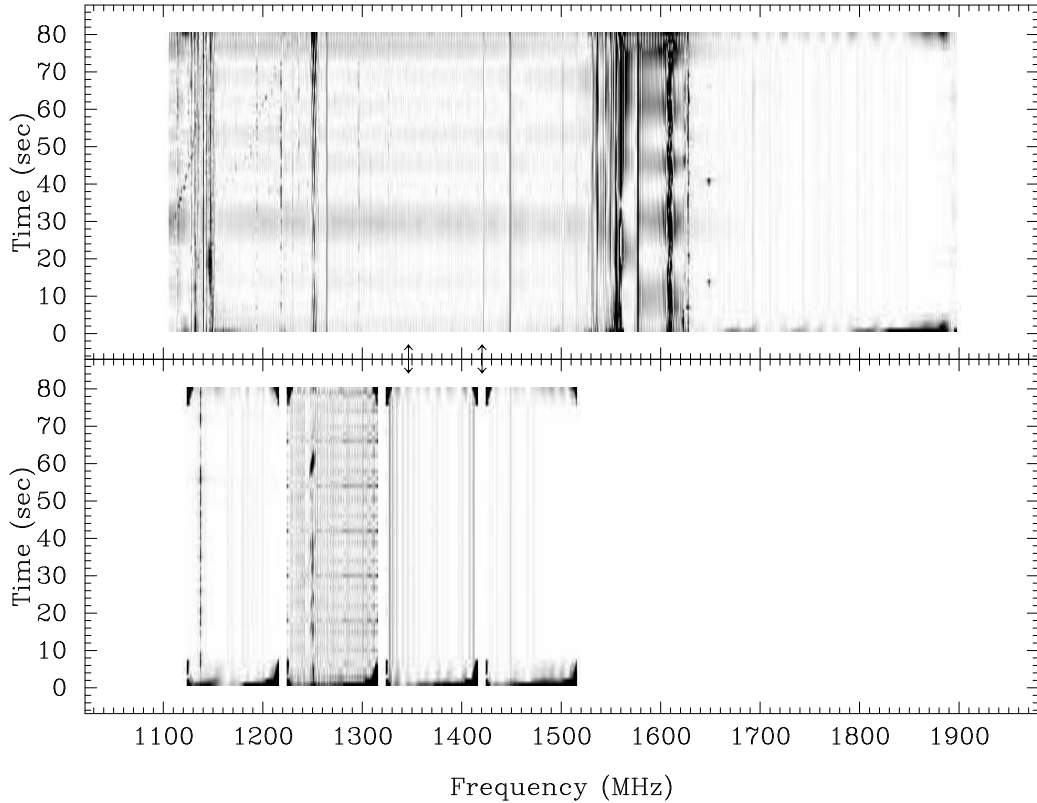


Figure 6. Gray scale plots showing the RFI-corrupted regions of the data taken on UGC 2339. The strength of the RFI is shown on a logarithmic gray scale, saturating (black) at 1.5 dB above the median power level. Different types of RFI can be seen, ranging from persistent RFI confined to a small frequency range to those that are bursty and strong (e.g. Iridium line). The top panel shows the GBT-SPIGOT data, while Arecibo-WAPP data are shown in the bottom panel. Locations of the unseen HI emission from UGC 2339 (at 1346.5 MHz) and that of the Galactic HI emission (at 1420.4 MHz) are indicated by two-sided arrows in the figure.

schemes for possible real signals. A detailed implementation of such an algorithm is beyond the scope of this paper.

The above scheme offers the choice of several control parameters that can be optimized to yield the best results. These include the window for median filtering, thresholds adopted at various stages of the algorithm and the number of iterations performed. The size of the median filter window is largely dictated by the resolution of data (in time and frequency), and the types of RFI that are present in the data. Our trials suggest use of a 5x5 window (i.e. the pixel under consideration is replaced by the median of all 25 elements in the 5x5 square neighborhood box in the time-frequency plane, including the diagonal elements) as an optimal choice to obtain the best results for the data taken with the SPIGOT

and WAPP spectrometers. We also emphasize that our use of a median filter is merely to identify RFI-corrupted intensity samples in the data, and hence it does not alter any statistical characteristics of the original data. The choice of thresholds can be based either on the statistics of the data samples, or in terms of a percentage increase of the mean bandpass level. Finally, the number of iterations influences the quality of RFI excision; for example, the use of fewer iterations may potentially result in some residual unexcised RFI in the data, the extent of which may serve as a useful figure of merit to assess the quality of RFI excision for a given set of parameters. As an end product, the algorithm effectively generates two-dimensional RFI “masks” which can be inputted to the various data processing pipelines.

In general, the choice of optimal thresholds and number of iterations will depend on the degree of

RFI contamination. For the data sets shown in Figs. 3–6, we find typically 3 to 4 thresholding passes (i.e. 1-2 to identify and excise spectral channels of persistent RFI, and the remainder 1-2 for the RFI-corrupted sections of data in the time-frequency plane) to be sufficient for eliminating a large fraction of the RFI. Generally, in our case most narrowband RFI are eliminated by using a threshold of 0.2 to 0.6 dB (i.e. 5 to 15%) above the median power level, while a threshold of $3\text{--}4\sigma$ seems to work well for RFI-excision in the two-dimensional time-frequency plane. We however emphasize that the choice of thresholds and number of passes are, in general, largely dictated by the spectrometer and receiver combination. Thus the optimal scheme for RFI excision may differ for the data taken with a different receiver or telescope and/or using a different spectrometer backend.

3.1. Extension to Dual-station Data

As stated in the previous sections, one of the original goals of these demonstrator observations was to exploit the dual-site nature of the data for its effectiveness to do better spectroscopy, especially in re-

gions of the band heavily contaminated by RFI. We applied the above-described RFI-excision algorithm on the UGC data set from each telescope separately, in order to examine the difference in the RFI environments at the two telescopes. Figure 6 shows the degree of RFI contamination at the two telescopes as a function of time and frequency for the data sets of UGC 2339. As seen from the figure, the RFI environment is relatively cleaner at Arecibo in the lower 100 MHz of the band, while it is considerably worse in the adjacent 1220–1320 MHz range. In general, RFI is seen to be largely uncorrelated between the two telescopes, and in principle, such uncorrelated RFI can easily be identified and excised using dual-site RFI mask data generated by the algorithm. For this galaxy, the HI emission is expected near 1346.5 MHz with a line width of approximately 2.1 MHz. Its apparent lack of detection in our data can be attributed to insufficient data length and coarse spectral resolution (0.781 MHz). However the data reveal the presence of 21 cm emission (at 1420.4 MHz) due to our own Galaxy.

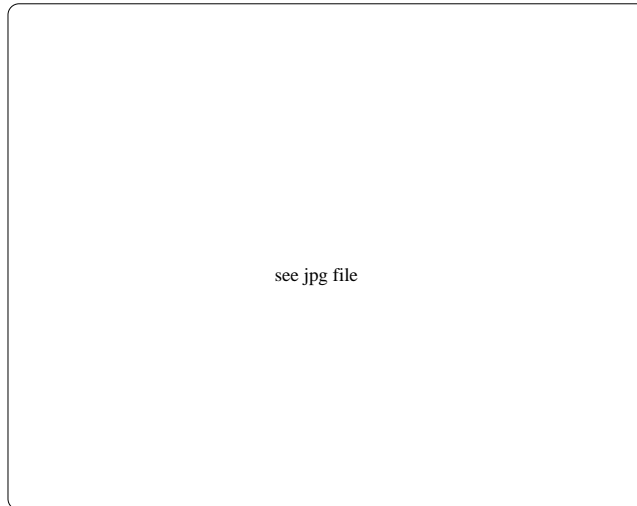


Figure 7. Schematic illustration of the transient event (e.g. giant pulse) detection method described in § 4.1. Data at the full resolution (in time and frequency) are converted into dedispersed time series, and searched for possible “events.” The event lists from multiple sub-bands or multiple sites can be compared to differentiate real events from spurious ones due to RFI.

4. Transient Detection in Time Series Data: RFI vs Real Events

Detection of transient signals is an important science goal for several upcoming and planned large telescopes such as the ATA, LOFAR, the Mileura Wide-field Array (MWA), the LWA, and the SKA, all of which are planned to have relatively wide fields of view, a key requirement for transient search. The Crab pulsar emits “giant pulses,” radio bursts whose amplitude can exceed the average pulse amplitude by orders of magnitude (e.g., Lundgren et al. 1995, and references within). There have been a variety of recent attempts to search for giant pulses from both Galactic and extragalactic objects (McLaughlin & Cordes 2003; Johnston & Romani 2003). One major difficulty with these searches is the prevalence of impulsive RFI, which often mimics giant-pulse-like signals in the time series data. Strong RFI can also potentially mask even the characteristically dispersed pulses from pulsars. Most new generation telescopes will offer unique means of circumventing this problem, via use of multiple sites and/or simultaneous multiple beams.

Our demonstrator observations described in § 2 are well suited for the exploration and development of techniques that could help discriminate between real signals and impulsive RFI. Specifically, our data taken on the Crab pulsar provide an excellent test bed for this purpose. We describe the single-pulse (giant-pulse) search method (Cordes & McLaughlin 2003) as an example of transient event detection schemes applicable to fast-sampled data (see Fig. 7), and demonstrate the leverage of dual-site and multiple-subband approaches for discriminating “real events” from those that are caused by impulsive RFI.

4.1. Transient Event (Giant Pulse) Detection in Fast-sampled Data

The single-pulse (giant-pulse) search method used for our analysis (Fig. 7) is essentially the same as that described in Cordes & McLaughlin (2003) and used by Cordes et al. (2004). The raw data are first converted into a filterbank stream, retaining the original resolution in time and frequency. These are then dedispersed by summing over frequency channels while taking into account time delays associated with plasma dispersion in the interstellar medium (ISM). The dedispersion is performed at one or many

dispersion measures (DMs) depending on whether the object is of a known DM (e.g. the Crab pulsar) or unknown DM. Often knowledge of the DM range expected toward an object (e.g. 60–80 pc cm⁻³ toward the M33 galaxy; Cordes & Lazio 2002) may help to narrow down the search in the DM parameter space. For reference, similar analysis is also performed for the case DM=0.

The dedispersed time series data are first analyzed with the original time resolution, and then progressively smoothed and decimated by factors of two in order to approximately match filter to pulses with different widths. Individual pulses (i.e. events) and their occurrence times are then identified by selecting intensity samples that exceed the mean level by a specified threshold (e.g., 3 to 5 σ). This process can (optionally) be performed iteratively by excluding the detected events (or the corresponding intensity samples) from previous iterations, until no more events are detected. These identified events can then be examined for detailed characteristics such as their strength, spatial grouping, time-frequency signature, etc.

While the above method appears to be effective to search for giant-pulse-like events from objects with known DMs, identification of real events becomes more difficult owing to false positives for the more general case of an unknown DM and an unknown type of signal, for which many more statistical trials must be done. In the remainder of the section we illustrate the leverage of some simple-minded, yet powerful methods of discriminating real events from spurious ones that may be generated by RFI.

4.1.1. Dual Station Technique

This is the simplest possible illustration of a more general multiple-site based approach that can potentially be used to differentiate real events from spurious ones caused by RFI. Assuming that much of the RFI is largely local to the site, and consequently likely to be uncorrelated between the two sites, a simple technique such as examining for coincidence vs anti-coincidence of the detected events can be used to filter out the events that are more likely to be real. In order to apply this method, it is essential that data from the two telescopes be processed in an identical manner, and that identical criteria are applied for the generation of event lists. The times of occurrence of the events are corrected for (a) any dispersion delays due to differences in the reference frequencies used for the dedispersion process; (b) any

instrumental delays; and (c) differences in the arrival times of the signal at the telescopes, before attempting the comparison. The events are then examined for the simultaneity as well as similarity in terms of properties, and those that are unambiguously detected by both the telescopes are categorized as likely real events.

Despite its simplicity, there are some caveats for this method. As the signal-to-noise ratio (S/N) of a detected event depends on the sensitivity of the instrument, it is quite possible many real events with only marginal detections at the more sensitive telescope may be classified as spurious ones. Such ambiguity can be minimized by appropriate scaling of the detection thresholds for uniformity of the detection criteria in terms of, for example, the minimum detectable flux density. Figure 8 shows an example segment of dual-station time series data of the Crab pulsar; both data sets show several large-amplitude spikes. Using the simplest criterion that “events” must appear in both data sets to be considered real (i.e. giant pulses), we identify a few spurious events in the GBT data that are likely caused by impulsive RFI. Further, the pulse-amplitude ratios appear to be slightly different for the two data sets, and this is most likely due to the difference in spectrom-

eter bandwidths (400 and 800 MHz respectively for the Arecibo and Green Bank data). For data sets of identical bandwidths, the pulse-amplitude ratios match within a few percent level.

4.1.2. Multiple Subband Technique

This method is especially suitable for observations that employ large spectrometer bandwidths (Arecibo’s WAPP and the GBT’s SPIGOT are good examples). In such cases, the RFI environment may vary considerably across the frequency range of observation, ranging from relatively clean parts of the band with little or minimal RFI to those that are marked by a highly RFI-rich environment. Often strong and bursty types of RFIs can potentially mask even the brightest giant pulses from Crab-like pulsars. Although this can be addressed in principle (or at least minimized) by the application of suitable RFI identification and excision algorithms (such as the one presented in § 3) prior to processing, and the integration of the generated RFI “masks” into the data reduction pipeline, such schemes may also be computationally expensive, especially when dedispersion needs to be performed over many trial DMs. With some trade-off in the achievable sensitivity for the event detection, an alternative scheme that makes use of multiple sub-bands (preferably equally-sized)

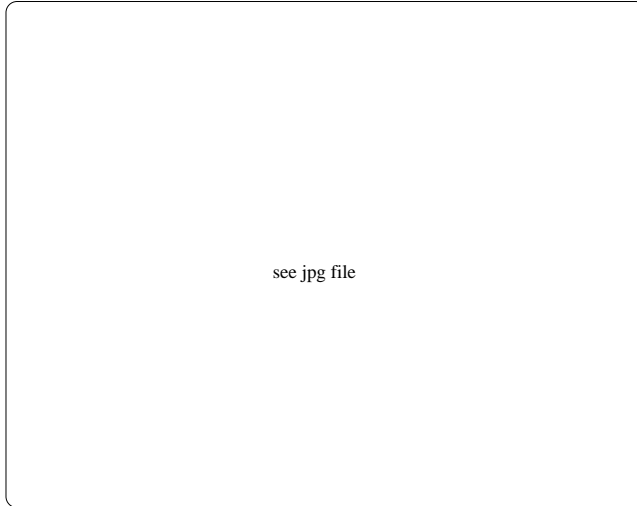


Figure 8. Dedispersed time series of the Crab pulsar from the Arecibo-Green Bank observations at L-band; data shown are for a short duration of 8 s. The top panel is the Arecibo data and the bottom one is the GBT data. Locations of the detected events (in Green Bank data) are indicated by the upward arrows; the events that are common to both the data sets correspond to positive identifications of giant pulses, and those that are unlikely to be real are marked by the ‘?’ symbol.

can be applied to such data. The data are split into several contiguous sub-bands, each of which is processed individually for application of the event detection algorithm. The multiple event lists generated in this manner are then examined for simultaneity (i.e. coincidence vs anti-coincidence approach between sub-bands), as well as similarity of the properties, after taking into account the time delay due to differences in the reference frequencies used for dedispersion. The events that have correspondence in two or more sub-bands are then classified as likely real events.

We illustrate this scheme using example data sets taken on the Crab pulsar in the frequency range from 1120 to 1520 MHz with the Arecibo WAPP system. In this case, four identical units of the multi-WAPP system, each capable of a maximum of 100 MHz bandwidth—spanning a total of 400 MHz band—make a logical split of the data into four contiguous sub-bands. Data from the four sub-bands are processed separately using a uniform set of event detection criteria in order to generate the respective event

lists, which are shown in Fig. 9. Clearly, the number of detected events (for an assumed 10σ threshold) is a strong function of the level of RFI contamination within the band, resulting in nearly two orders of magnitude larger number of events in the WAPP unit that spans the 1220 to 1320 MHz range (see also Figs. 1 and 3). Examination of these event lists for simultaneity or correspondence between different sub-band pairs yields a much fewer number of events that are common. In fact the least number of events is detected for the combination that includes the RFI-rich band (1220–1320 MHz) of WAPP2. A plausible reason for such a disparity may be an apparent increase in the noise rms resulting from the high degree of RFI contamination, leading to many real events escaping through the event detection algorithm.

Despite its simplicity and demonstrated success, some consequences and caveats are in order for this method. First, this apparent efficiency comes at the cost of somewhat larger processing requirements; i.e. N data streams to deal with at the post-dedispersion

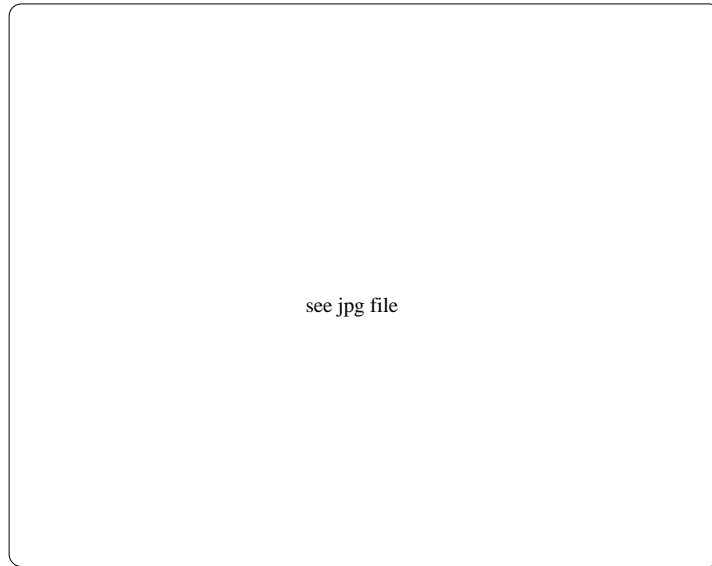


Figure 9. Time series of “events” (i.e. plots of S/N vs sample number) detected by the single-pulse detection algorithm as described in § 4.1; top to bottom panels on the left correspond to 100 MHz bandwidth chunks spanned by four units of the WAPP, i.e. WAPP1 (1120–1220 MHz), WAPP2 (1220–1320 MHz), WAPP3 (1320–1420 MHz) and WAPP4 (1420–1520 MHz). Right panel: coincident events (green) for the different sub-band pairs WAPP1-WAPP2, WAPP1-WAPP3 and WAPP1-WAPP4 (top to bottom), overplotted on the time series of events detected in the WAPP1 sub-band (left, top panel).

stage (where N is number of sub-bands), and in the case of many-DMs, this implies roughly N -fold increase in processing requirements. Further, some caution is needed in the interpretation of uncorrelated or partially correlated events between different sub-bands. For example, diffractive interstellar scintillations modulate the frequency structure of intensity at a given time, and this may potentially lead to apparent lack of simultaneity of real events. Indeed some knowledge of the expected scintillation bandwidth (predictable for a given DM and line of sight with some reasonable accuracy) can be integrated into event detection criteria. For instance, the Crab pulsar is known to show scintillation structures $\lesssim 1$ MHz bandwidth at L-band frequencies (Cordes et al. 2004). Moreover the scintillation characteristics vary with the epoch of observation. This can potentially be addressed by use of more complex and stringent criteria for filtering out real events, such as a simultaneity check of events in more than two sub-bands, and possibly between multiple sites. In any case, this method illustrates a feasible and efficient scheme that can be applied to data from wide-bandwidth observations.

5. Summary and Conclusions

We have developed and tested an algorithm for identification and excision of RFI in fast-sampled spectrometer data. The basic principle involves the application of a two-dimensional median filter, followed by a series of thresholding and excision performed in stages, and possibly in multiple passes, to yield the best results. The method is sensitive to a wide variety of RFI and can be used to generate RFI masks for input into applications such as pulsar data processing or spectroscopy in bands heavily contaminated by RFI.

The prevalence of impulsive RFI has long been recognized as a major difficulty in transient event detection schemes applicable to time series data. Using data from our recent Arecibo-Green Bank simultaneous observations (L band) of the Crab pulsar, we have explored effectiveness of multi-site and multi-subband approaches to help discriminate between real events and the spurious ones due to RFI. The basic idea involves examining the coincidence vs anti-coincidence of detected events after taking into account the dispersion, instrumental and other delays. The subband technique appears to be efficient

for filtering out real signals from the likely forest of events in the sub-bands with RFI-rich RFI environments. In general the combination of multiple-site and multiple-subband offers great promise in this arena. Applications to specific science goals, such as detections and searching for giant pulses and other fast transients, are deferred to a subsequent paper. This will make use of our existing dual-site data on Crab and M33, as well as data from future such observations and the upcoming multibeam pulsar surveys at Arecibo.

Acknowledgments. We are grateful to Karen O’Neil and David Kaplan for all their guidance and assistance in the planning and conducting of these observations, and to Scott Ransom for the PRESTO software package which was used for the initial analysis of these data. This work was supported by NSF grant AST 0138263 to Cornell University for technology development for the SKA. The Arecibo Observatory is operated by Cornell University under a cooperative agreement with the NSF. The National Radio Astronomy Observatory is a facility of the NSF operated under cooperative agreement by Associated Universities, Inc. NDRB is supported by an MIT-CfA Fellowship at Haystack Observatory. Basic research in radio astronomy at the NRL is supported by the Office of Naval Research.

References

- Cordes, J.M., Bhat, N.D.R., Hankins, T.H., McLaughlin M.A. & Kern, J. (2004), The Brightest Pulses in the Universe: Multifrequency Observations of the Crab Pulsar’s Giant Pulses, *ApJ*, 612, 375.
- Cordes, J.M. & Lazio, T.J.W. (2002), NE2001.I. A New Model for the Galactic Distribution of Free Electrons and its Fluctuations, *ApJ*, Submitted, Astroph/0207156.
- Cordes, J. M. & McLaughlin, M. A. (2003), Searches for Fast Radio Transients, *ApJ*, 596, 1142.
- Johnston, S. & Romani, R. W. (2002), A search for giant pulses in Vela-like pulsars, *MNRAS*, 332, 109.
- Lundgren, S.C., Cordes, J.M., Ulmer, M., Matz, S.M., Lomatch, S., Foster, R.S., & Hankins, T. (1995), Giant Pulses from the Crab Pulsar: A Joint Radio and Gamma-Ray Study, *ApJ*, 453, 433.
- McLaughlin, M. A. & Cordes, J. M. (2003), Searches for Giant Pulses from Extragalactic Pulsars, *ApJ*, 596, 982.
- Ransom, S. M., Stairs, I. H., Backer, D. C., Greenhill, L. J., Bassa, C. G., Hessels, J. W. T., & Kaspi, V. M. (2004), Green Bank Telescope Discovery of Two Binary Millisecond Pulsars in the Globular Cluster M30, *ApJ*, 604, 328.

(Received _____.)

This figure "f2.jpg" is available in "jpg" format from:

<http://arxiv.org/ps/astro-ph/0502149v1>

This figure "f5.jpg" is available in "jpg" format from:

<http://arxiv.org/ps/astro-ph/0502149v1>

This figure "f7.jpg" is available in "jpg" format from:

<http://arxiv.org/ps/astro-ph/0502149v1>

This figure "f8.jpg" is available in "jpg" format from:

<http://arxiv.org/ps/astro-ph/0502149v1>

This figure "f9.jpg" is available in "jpg" format from:

<http://arxiv.org/ps/astro-ph/0502149v1>